Journal of Molecular Liquids 362 (2022) 119631

Contents lists available at ScienceDirect

Journal of Molecular Liquids

journal homepage: www.elsevier.com/locate/molliq

PPDN and NTCDA radical anions formation in EMIM-DCA, BMIM-BF_4 EMIM-Ac ionic liquid solutions under the steady state UV and Vis light illumination: A combined X-, K-band EPR and DFT study

A. Konkin [a,*], U. Ritter [a], A.A. Konkin [a,b], A. Knauer [a], V.I. Krinichnyi [c], V. Klochkov [b], A. Aganov [b], M. Gafurov [b], F. Wendler [d], P. Scharff [a]

[a] Institute of Micro- and Nanotechnologies MacroNano®, Technische Universität Ilmenau, Gustav-Kirchhoff- Str.7, D-98693 Ilmenau, Germany
[b] Institute of Physics, Kazan Federal University, Kremlyovskaya Str. 18, Kazan, Russia
[c] Department of Kinetics and Catalysis, Institute of Problems of Chemical Physics RAS, Academician Semenov Avenue 1, 142432 Chernogolovka, Russia
[d] TITK, Smartpolymer GmbH, Breitscheidstraße 97, 07407 Rudolstadt/ Thuringen, Germany

ARTICLE INFO

Article history:
Received 21 December 2021
Revised 11 May 2022
Accepted 14 June 2022
Available online 24 June 2022

ABSTRACT

The radical anion of Pyrazino[2,3-f][1,10]phenanthroline-2,3-dicarbonitrile (PPDN) in blends with imidazolium based room temperature ionic liquids (RTIL): EMIM-DCA, BMIM-BF_4, EMIM-Ac has been detected by X-band continues wave (CW) electron paramagnetic resonance (EPR) under steady state Xe-lamp illumination in the temperature interval from 190 to 340 K. The radical anion of 1,4,5,8-Naphthalenetetra carboxylic dianhydride (NTCDA) was registered by X- and K-band CW EPR at room temperature under the visible light CW diode laser operated at 532 nm, and Xe-lamp as well. The experimental hyperfine coupling data of both anion radicals were confirmed by DFT calculation. The formation of $PPDN^{\bullet-}$ $NTCDA^{\bullet-}$ and fullerene derivative (FD) radical anions is attributed to the photoelectron transfer from an IL anion to PPDN, NTCDA and FD electron acceptors. Here, the electron transfer leads to an irreversibility of these reactions due to photo-induced decomposition of the IL anions in the presence of an effective electron acceptor and is supported in the above RTILs solutions by means of EPR. For the indirect confirmation of the EMIM-DCA, EMIM-AC, BMIM-BF_4 anion degradation in solutions with PPDN and NTCDA up to the transient radical state, similar data of acetate anion $[OCOCH_3]^-$ decomposition, under CW Xe-Lamp photolysis resulting in $CH_3^{\bullet}$ formation and its stabilization at 77 K in EMIM-Ac suspension with some FD dissolved in DCB are introduced as well. However, the main goal of this study is dedicated to the features of rotational and translational diffusion kinetics of PPDN and NTCDA radical anions in IL solutions as well to the evaluation of their application as a spin probes in ILs study in liquid phase.

© 2022 Elsevier B.V. All rights reserved.

1. Introduction

The exceptional physicochemical properties of widely used room temperature ILs (RTIL), such as low melting point and vapor pressure, electrochemical and thermal stability, a wide electrochemical window, as well as good conductivity, lead to a stable and constant growth of interest from the side of researchers and industry [1,2]. RTILs relate in general to green solvents [3], however, it mainly could be assigned to their low vapor pressure [4]. An increasing usage of ILs certainly increases the probability of the appearance of their decomposition products in environment. Therefore, it is rather important to have data concerning stability and breakdown products of the ILs and knowledge about possible decay processes of those IL compounds, at least for the abiotic transformation within technical applications [5]. With respect to biotic processes with IL participation, the toxicological influence of possible products of RTIL degradation should be the priority in focus [6]. While the main data concerning ILs thermo-, hydrolysis-, photo- and radiolysis stabilities seems to be sufficiently represented in the literature, for example [7,5,8], the exclusive photo-degradation reactions in the presence of electron acceptors (*EA*), need additional studies. This supposition is based on the experimental data of a relatively easy photo-induced decomposition of some organic anions, and was specified by an electron transfer from the IL anion to the *EA* molecule in solution. For instance, a photochemical reaction between C_{60} fullerene and anions of tetraphenylborate and triphenylbutylborate via photoelectron transfer results in the formation of fullerene radical anion ($C_{60}^{\bullet-}$) and radicals $^{\bullet}BPh_3R$ (R = Ph or Bu) that was detected under

* Corresponding author.
E-mail address: alexander.konkin@tu-ilmenau.de (A. Konkin).

https://doi.org/10.1016/j.molliq.2022.119631
0167-7322/© 2022 Elsevier B.V. All rights reserved.

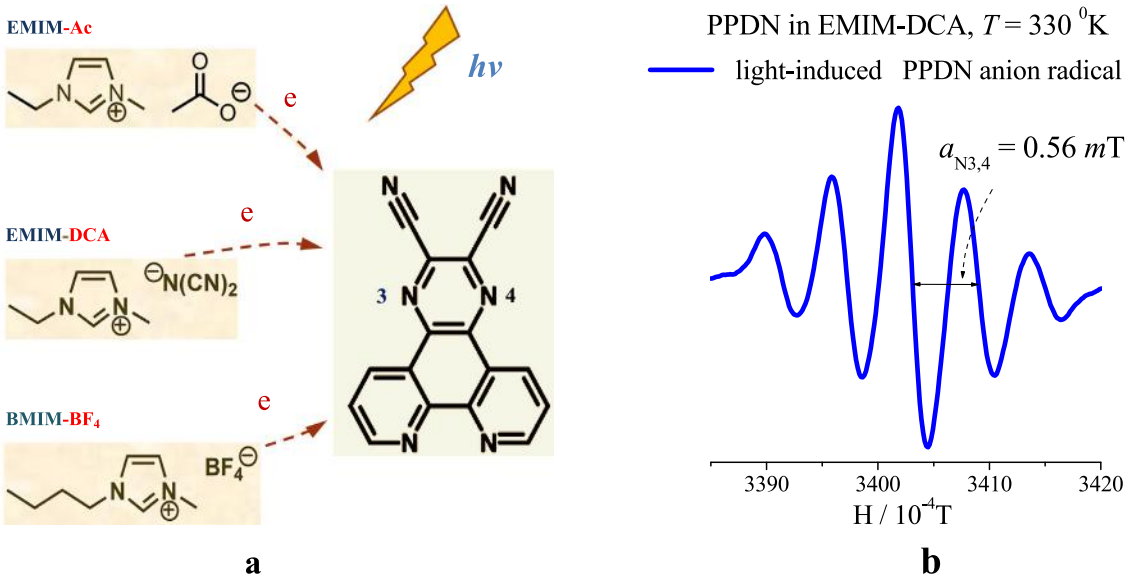

Fig. 1. a) Utilized RTILs: IMIM-DCA, IMIM-Ac, BMIM-BF_4 and PPDN structures with electron transfer path from IL anions to PPDN under light excitation, b) EPR spectrum of PPDN anion radical ($PPDN^{\bullet-}$) in EMIM-DCA recorded at T = 300 °K.

continuous wave (CW) and pulse excitation [9]. Note that the above mentioned borate radical products have been detected under the CW light illumination by Xe-Hg lamp (150 W) with a light source output power density of just several tens mW/cm^2, at the sample place of the ESR resonator cavity. With regards to the ILs/RTILs stability under CW light excitation, it was reasonable to check RTILs anions, as potential sources of photoelectrons in the presence of some *EA*s including FDs, taking in mind that this photoreaction can lead to an irreversible degradation of the IL. The data concerning a short-living radical transient state of electron transfer process in electron donor/acceptor systems, included RTIL anions as electron donors, has been obtained recently, using time-resolved absorption spectroscopy [10,25]. The data concerning the direct radical formation in RTIL under high power pulse radiolysis and photolysis are known to literature, for instance [8] and its references. In case of the essential anisotropy of radical anion (RA) EPR parameters (hyperfine coupling constants (*hfc*), and g-tensor), one can consider some *EA*s (or RAs) diluted in the IL as sensitive spin probes (*sp*) for RTIL studies, at least when common tasks regarding the diffusion of charged species as well as the kinetics of generation and recombination of the light induced radical anions (LIRAs) in RTILs are in the focus of the study. Indeed, the systematic investigation of molecular rotational diffusion in RTILs utilizing a stable spin probe is certainly attributed to nitroxides, mainly mono-radicals, as well as their charged derivatives for instance [11–23]. However, in our case, the light-induced radical anions (LIRAs) are the species with a light-dependent/guided concentration and their negative charges are not stabilized by the metal counter-ions in contrast to the charged nitroxide radicals with anionic substituents, for instance, K^+, Na^+ [13,15]. LIRAs are relatively stable species and in principle could be considered as the long lived electron donors in possible blends, consisted RTILs. EPR enables to study diffusion processes and the corresponding kinetics of LIRAs formation/annihilation reactions in ILs. Therefore, the search of additional *sp* like LIRAs to the charged nitroxides family makes sense for some tasks, for instance, the study of the kinetics of chemical exchange reactions between LIRAs and it's precursor in ILs, i.e. *EA* molecule. Furthermore, the specific influence of the decay products as well as of the generated radicals on biological objects should be investigated. This supposition is based on the data concerning thiocyanate $(SCN)^{\bullet}$ radicals' contribution in DNA damage [24], as well as its possibility to potentiate antimicrobial photodynamic therapy [25]. With regard to the IL, note that the precursor of $(SCN)^{\bullet}$ is the $(SCN)^-$ anion in the according photo oxidation reaction, which is a component of the widely used RTIL (namely IMIM-SCN). Thus, it seems to be reasonable to expect similar properties from other IL anions, for instance, DCA and Ac, in IMIM-DCA, IMIM-Ac.

2. Experimental

Three imidazolium-based RTILs from Ionic Liquids Technologies (IoLiTec) GmbH (Germany), have been used in this study: 1-butyl-3-methylimidazolium tetrafluoroborate BMIM-BF_4, > 99%; 1-Ethyl-3-methylimidazolium dicyanamide, >98%, 1-Ethyl-3-methylimidazolium acetate EMIM-Ac, 95%. PPDN was purchased from Luminescence Technology Corp. (Hsin-Chu, Taiwan) > 98%, NTCDA in Merck. The samples for EPR experiments were prepared as PPDN and NTCDA filtered solutions in EMIM-DCA and BMIM-BF_4 with the concentrations of $(0.5–6)\cdot10^{-3}$ mol/*L*. However, the comparison of EPR spectra of the filtered and unfiltered solutions does not indicate an influence of a possible residual undiluted solid state fraction of *EA* with particles sizes < 0.2 μm at the *hfc* line changing as shown in Fig.S9 in SM-3a. The measurements were carried out in the temperature range between 220 and 363 °K and at 77 K for FD-BN:EMIM-Ac suspension, however the top boundary (up to ~ 360 °K) refers to the solutions of PPDN and NTCDA in BMIM-BF_4. The *X*- and *K*-band EPR spectra were recorded using a CW Bruker spectrometer ELEXYS E500 operated at ~ 9.4 GHz / 0.34 T (X-band) and ~ 24 GHz/0.83 T (*K*-band) microwave frequency. For the light excitation of PPDN solutions and FD suspensions, an Osram XBO 150 W Xe-lamp was utilised, while for NTCDA solutions a 50 mW diode laser at 532 nm for the CW photolysis has been used. An optical transmission resonator, ER 4104OR (Bruker BioSpin), provided a simple pathway for the Xe-lamp light (~30 mW/cm^2) in X-band EPR studies. For the K-band experiments with NTCDA solutions, an attachment, based at a hollow thin-walled nonmagnetic metal cylinder (750 mm long, and 7 mm in diameter) was developed for the direct coaxial passage of the laser beam inside the cylinder of the K-band resonator. To exclude undesirable line broadening connected with the saturation and over-

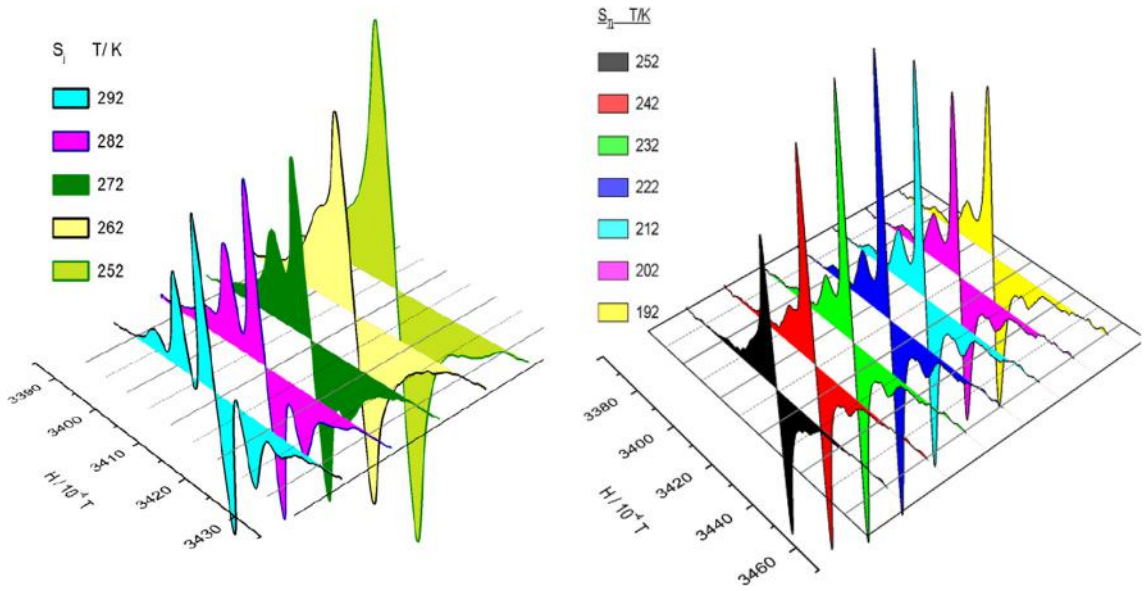

Fig. 2. PPDN$^{-\bullet}$ spectra in EMIM-DCA solution recorded below and higher of the freezing temperature T_f = 252 K: a) T_i > 252 K, and b) below T_j < 252 K.

modulation of narrow EPR spectra in NTCDA solutions, the microwave power $P_{\mu w}$ and magnetic field modulation amplitude H_m in the most of experiments attributed to ESR linewidth study were not exceeded 0.5 mW and 0.02 mT respectively.

3. Results and discussion

The study of anion radical formation in IL blends with potential organic electron acceptors (*EA*) we have started before in blends like suspension of EMIM-Ac and fullerene derivative solution in o-DCB and the main results are exhibited in SM-1. The decomposition of acetate (Ac) anion $(OCOCH_3)^-$ in EMIM-Ac due to charge/-electron loss was detected in the presence of FD as *EA* of photo-induced electrons under CW Xe-lamp excitation even at low temperatures with the light power density at about several tens of mW/cm^2. Note, that without FD, the radical products number, accumulated under the same conditions of illumination and registration, in our experiments does not exceed 4% of those obtained with *EA*. The photo-induced reaction of the decomposition of $(OCOCH_3)^-$ in EMIM-Ac at transient state and with experimentally stabilized radical products due to the low temperature of 77 K can be written as:

$$[OCOCH_3]^- + h\nu \rightarrow {}^{\bullet}OCOCH_3 + e^-$$

$$^{\bullet}OCOCH_3 \rightarrow CO_2 + {}^{\bullet}CH_3$$

$$EA + h\nu \rightarrow {}^{*}EA \rightarrow {}^{*}EA + e^- \rightarrow EA^{\bullet -}$$

where the photoelectron initiates the same path-way of Kolbe reaction in the intermediate state, as an anode in the electrolysis of an acetate anion [26]. The detailed data of EMIM-Ac:FD photolysis: FD structures and EPR spectra analysis are introduced in § SM-Iab.

4. PPDN

With respect to the photochemical reaction, which is initiated by photoelectron transfer, the obtained here basic data are given in Fig. 1 in a rather compressed form. The anions of the above RTILs lose electrons under light excitation and the photoelectron is trapped by a suitable organic *EA* (here PPDN), dissolved in IL. The result of the photoreaction is the formation of the relatively stable anion radical PPDN$^{-\bullet}$. Since, at transient state, the mechanism of radicals generation in those blends, is the same due to photoelectron transfer from IL anions [10,27], this resulting the formation of short living active neutral radical A$^{\bullet}$ of anion molecule A$^-$ and more stable anion radical of the EA (C$^+$ -cation of IL).

$$(C^+\text{-}A^-) + EA + h\nu \rightarrow C^+ + A^{\bullet} + e + EA \rightarrow C^+ + A^{\bullet} + EA^{\bullet -}$$

The designation of cation-anion (C+ - A$^-$) abbreviations in IL by signs (+, -) is used here only in the above reaction scheme and is omitted in all other places of this work. With regards to DCA$^-$ composed in IL, the photo- induced decomposition of the DCA$^-$ anion due to electron loss has been detected via the registration of intermediates DCA$^{\bullet}$ and $(DCA)_2^{\bullet -}$ [10,27] radicals by means of time-resolved absorption spectroscopy after an excitation by the flash photolysis or radiolysis, however we expect the above intermediate transient radicals states formation under CW light in the presence of *EA*.

$$DCA^- + h\nu \rightarrow DCA^{\bullet} + e^-$$

$$DCA^{\bullet} + DCA^- \rightarrow (DCA)_2^{\bullet -}$$

An example for an EPR spectrum, recorded at 42 °C, with the resolved hyperfine structure, that is attributed to unpaired electron spin coupling with two nuclear spins of equivalent nitrogen ($N_{(3,4)}$, I = 2) is shown in Fig. 1b. The temperature experiments indicate that even at temperatures more than room temperature (T_R), the spectra show the dependence of hyperfine linewidths ΔH_m on the nuclear quantum numbers m = -2, −1, 0, 1, 2 of the effective nuclear spin I = 2 and demonstrate a clear change in the linewidth of hyperfine components as a function of temperature. The examples of appropriate EPR spectra in EMIM-DCA:PPDN solution, recorded in the temperature range 292 K – 252 K are shown in Fig. 2a,b and for detailed consideration, 2*D* format is repeated in Fig. S8 (SM-2e).

Therefore, the topic discussed below mainly concerns the possibility of using PPDN$^{-\bullet}$ as a light-induced EPR spin probe for studying problems of molecular diffusion in RTIL, as well as comparing the obtained data with data from the family of nitroxide radicals.

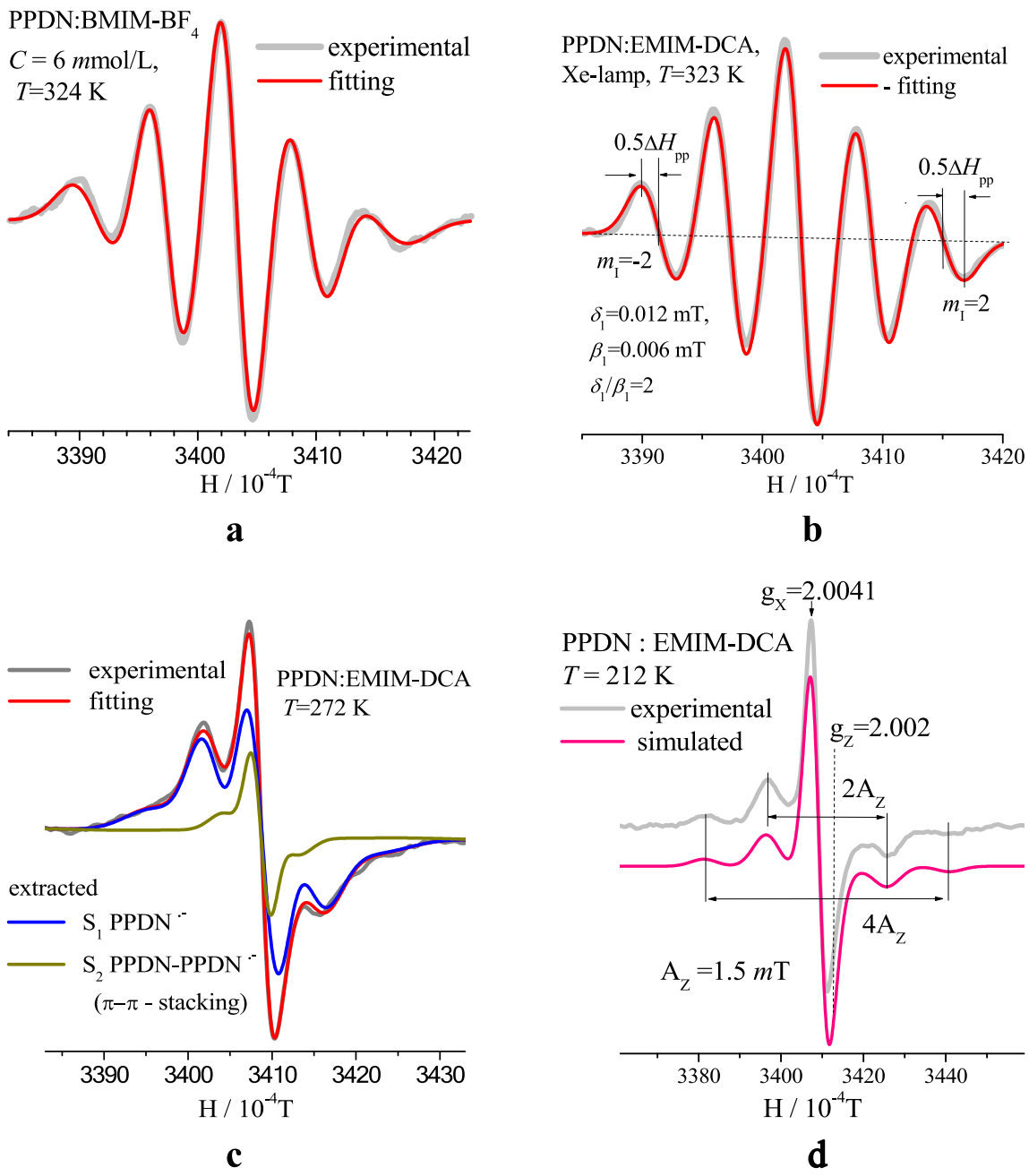

Fig. 3. PPDN$^{-\bullet}$ anion radical EPR spectra (I_{eff} = 2, multiplicity M = 2I + 1 = 5): a,b) experimental and fitted spectra of PPDN:BMIM-BF$_4$ and PPDN:EMIM-DCA solutions respectively, at T = 323 K, $A_{0N} \approx 0.56$ mT, c) in PPDN:EMIM-DCA solution, at T = 272 K, $A_{0N} \approx 0.52$ mT, $A_{01N} \approx 0.27$ mT for the set of two PPDN π-stacking (see SM-2b), d) experimental and simulated spectra of PPDN:EMIM-DCA recorded in solid state phase (frozen solution) at T = 212 K. We note that in the spectra processing/fitting procedure the base line has been set as a linear function.

In diluted solutions, one of the important relaxation mechanisms for spin doublets arises from motional modulation of the anisotropic Zeeman and the anisotropic nuclear-electronic *hfc*. The analysis of the different contributions to the individual *hfc* linewidths (ΔH_m), depends on the time-dependent correlation functions (*cf*) for the molecular orientations and for the molecular angular momentum [28,29]. Data of the *cf* correlation time (τ_c) dependence versus temperature can be obtained from the EPR spectra, namely $\Delta H_m = F(T)$ dependence described below by the expressions (1,1a) introduced below. The variation of ΔH_m arises from the modulation of the anisotropic *hfc*- and g- tensors, by rotational diffusion and can be expressed in the form given in [29], which is suitable for experimental EPR spectra processing.

$$\Delta H_m = \alpha_0 + (\alpha + m\beta + m^2\delta)\ \tau_C = \alpha_0 + \alpha_1 + m\beta_1 + m^2\delta_1 \qquad (1)$$

The parameters α_o, α, β, δ in expression (1) are discussed a bit later and τ_c is the correlation time in the Debye Stokes Einstein (DSE) theory of rotational relaxation, that can be given by the expression.

$$\tau_C = \frac{4\pi\eta R^3 C_S f}{3kT} = \frac{V\eta C_S f}{kT} \qquad (1a)$$

in which η is the viscosity coefficient, R is the molecular hydrodynamic radius of the equivalent rotating sphere with the volume V, f is referred to as a shape factor, C_S is the boundary condition parameter dependent on the solvent and the concentration, and k is the Boltzmann constant. In this work, Arrhenius-type relation-

Table 1
Hfc constants of "magnetic atoms" and g-tensor components of $PPDN^{-\bullet}$ evaluated by DFT.

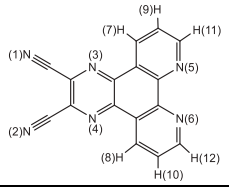

atoms	N(3,4)	N(1,2)	N(5,6)	H(7,8)	H(9,10)	H(11,12)
hfc						
A_0	**5.3**	0.29	−0.33	−0.51	−0.014	−1.02
A_{0exp}	**5.6**					
A_X	−0.33	−0.17	−0.1	0.48	0.15	−0.29
A_Y	−0.36	−0.20	−0.16	−0.88	−0.23	−1.1
A_Z	**15.8**	1.26	−0.7	−1.12	0.34	−1.66
A_{Zexp}	**15,6**					

g_x = 2.0040, g_y = 2.0037, g_z = 2.0021, g_0 = 2.0032

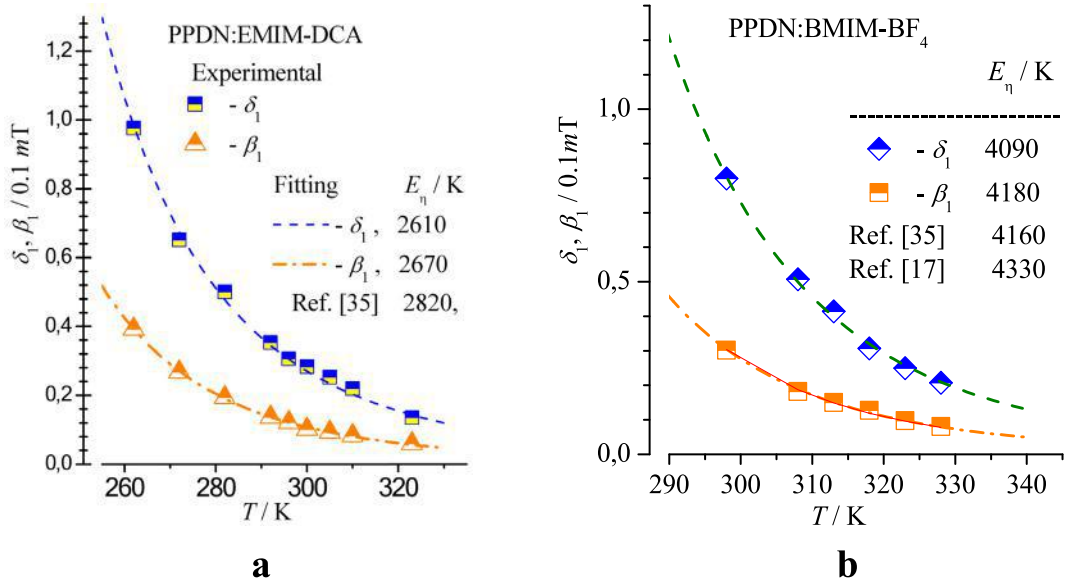

Fig. 4. Experimental β_1, δ_1 dependence versus temperature for: a) PPDN:EMIM-DCA and b) PPDN:BMIM-BF_4. Dashed lines are results of the fitting. In inserts: Arrhenius E_η [in K] are shown, which were obtained from the experimental data fitting (see text) and E_η taken for comparison from literature [35,17].

ship $\eta = \eta_\infty \exp(E_\eta/T)$ of viscosity as a function of temperature has been applied for $\tau_c = F(T)$ dependence analysis, where E_η (in Kelvin) is the apparent activation energy and η_∞ is the viscosity at infinite temperature. The parameters α_1, β_1, δ_1 in expression (1) were obtained via processing of experimental EPR spectrum by means of a least-squares method in each temperature point. The normal distribution of the integral intensity between the hyperfine spectrum lines (1:2:3:2:1) for two equivalent nuclear with spins I = 1 was assumed, namely the effective nuclear spin I_{eff} = 2 and the multiplicity M = 2I + 1 = 5. The processing of the EPR spectra has been carried out by.

$$Y = \sum_{j,\ m} (F_{(G,L)j}(H - H_{j,m},\ \Delta H_{j,m}) \qquad (2)$$

where the index j = 1,2 indicates the possibility of two different spectral contributions in solution, $F_{(G,L)}$ is Lorentzian or/and Gaussian, H_m is the resonance field of m-th *hfc* line and ΔH_m is the individual half-linewidth on the half maximum amplitude

In our case, the fitting of the $PPDN^{-\bullet}$ by means of a Gaussian line shape is in better agreement with the experimental spectra, due to the strong contribution of the inhomogeneous *hfc* line broadening, while in case of $NTCDA^{-\bullet}$ the combination of both X·Lorentzian+(1-X)·Gaussian is preferable (X is the relative contribution of the Lorentzian line shape function, and in our case is about 0.8). The examples of experimental and fitted spectra are shown in Fig. 3-a-d. With regards to the $PPDN^{-\bullet}$ in BMIM-BF_4 and EMIM-DCA solutions, the EPR spectra in Fig. 3a,b demonstrate a good correlation of fitted and experimental data with isotropic $A_{0N} \approx 0.56$ mT. However, in the EMIM-DCA solution at temperatures below 290 K, a better agreement with the experimental data has been achieved, assuming an additional contribution to the basic $PPDN^{-\bullet}$ spectrum for about 10% of the spectrum, which can be constructed by setting $A_{0N} \approx 0.26$ mT as shown in Fig. 3c. This supposition is attributed to the model of the effective electron hopping between $PPDN^{-\bullet}$ and neutral PPDN via pseudo-collision in case of relative positions of two planar molecules that are close to a π-π stacking architecture. The latter is related to the specific geometry of the collision, i.e. a steric factor. Thus, the ratio of the cross section of reactive collisions due to effective electron hopping in π-π-stacking PPDN-$PPDN^{-\bullet}$ to the total cross section of collisions is ~ 0.1. This version has been evaluated by DFT calculations with an optimization of the steric π-π stacking structure/energy as well an unpaired electron spin density distribution in two π- stacked PPDN molecules and the results are introduced in SM-2b. The calculation of the *hfc* constants of all $PPDN^{-\bullet}$ "magnetic" atoms was carried out by DFT/B3LYP/ 6-311G in ORCA [30] and the results are displayed in

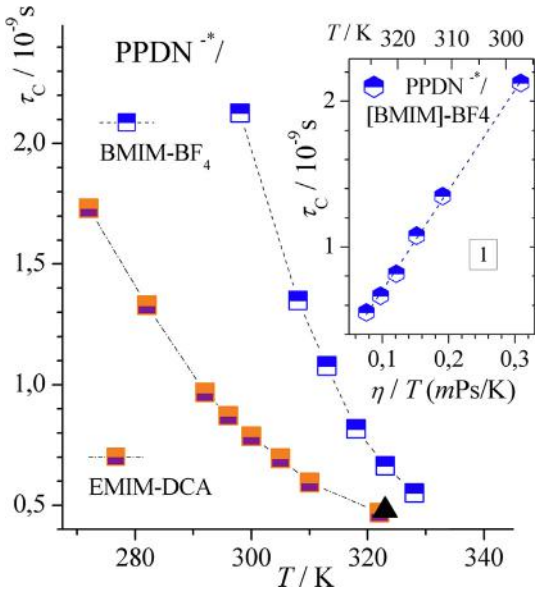

Fig. 5. Correlation time $\tau_c = F(T)$ of PPDN$^{-\bullet}$ in BMIM-BF_4, EMIM-DCA solutions. Insert **1:** $\tau_c = F(\eta/T)$ in BMIM-BF_4 solution. ▲ refers to the result of processing without spectrum fitting (as discussed in text).

Table 1. The comparison of the experimental and DFT data, shown in Table 1, displays a good coincidence for isotropic and anisotropic magnitudes of N(3,4) *hfc* parameters. This result hints for the fact, that the appropriate *hfc* parameters for other N_i, H_j atoms in Table 1, which cannot be resolved experimentally by EPR are close to the actual values. Regarding to the expression for α, β, δ in (1), the explicit data obtained experimentally and by DFT can also simplify the general expressions for $\Delta H_m \sim 1/T_2$ (T_2 is a usual denomination of the transverse relaxation time in magnetic resonance phenomenon).

In case of a triaxial anisotropy of the paramagnetic center, the parameters α, β, δ depend on anisotropic EPR parameters: g_z, g_x, g_y and A_z, A_x, A_y, [31].

With: $\Delta g = g_z - (g_x + g_y)/2$, $\Delta A = A_z - (A_x + A_y)/2$, $\delta g = (g_x - g_y)/2$, $\delta A = (A_x - A_y)/2$, $H_0 = h\nu/(g_0\mu_B)$ - resonance field, h – Planck constant ($h = h/2\pi$), $\omega = 2\pi\nu$ with $\nu = 9.4$ GHz (EPR microwave operating frequency), $g_0 = 1/3(g_x + g_y + g_z)$, μ_B - Bohr magneton. Taking in mind the DFT results displayed in Table 1, then it is possible to set in our case $A_x \approx A_y = A_\perp$, $\delta A = (A_x - A_y)/2 \approx 0$, $A_z = A_{//}$ and $\Delta A = A_z - (A_x + A_y)/2 \approx A_{//} - A_\perp \approx A_{//}$. The EPR parameters are close to the axial symmetry approach, however, with a strong axial anisotropy. Additionally, looking ahead to the experimental data represented below in Fig. 5, it can be stated concerning the range of the correlation time, i.e. $\tau_c \approx (0.5–2)\cdot10^{-9}$ s (including extreme values for both ILs in the appropriate temperature range), and an evaluation gives $1/[1+(\omega\tau_c)^2] \approx 1\cdot10^{-3} - 7\cdot10^{-5}$. Therefore, $\tau_c / [1+(\omega\tau_c)^2]$ in (3) can be neglected, and expression (3) can be written as.

$$T_2^{-1} = \frac{\tau_C}{5\hbar^2}\left[\frac{4}{9}(\Delta g H_0)^2\mu_B^2 + \frac{1}{8}\Delta A^2(3I(I+1)+5m_I^2) - \frac{4}{3}(\Delta g H_0)\Delta A\mu_B m_I\right] \quad (4)$$

or in terms of the linewidth ΔH_m, that is related to T_2^{-1} by the relationship T_2^{-1} (h /$g_0\mu_B$), one can overwrite eq.1 as follows.

$$\Delta H_m = T_2^{-1}\left(\frac{\hbar}{g_0\mu_B}\right) = \alpha_0 + (\alpha + m\beta + m^2\delta)\ \tau_C = \alpha_0 + \alpha_1 + m\beta_1 + m^2\delta_1 \quad (5)$$

where $\alpha = \left[\frac{4}{45}(\Delta g H_0)^2 + \frac{3}{40}\Delta A^2 I(I+1)\right]\ \gamma$, $\beta = \left(\frac{4}{15}\Delta A\Delta g H_0\right)\gamma$, $\delta = \left(\frac{1}{8}\Delta A^2\right)\gamma$ and

$\gamma = (g_0\mu_B)/$ h. In (5) $\alpha_0 = \alpha_{in} + \alpha_{ex} + \alpha_{dd} + \alpha_{hfc}$ is included: a) the individual linewidths (α_{in}) b) the "residual" linewidths attributed to unspecified mechanisms of line broadening for instance Heisenberg exchange (α_{ex}) and dipole–dipole interaction (α_{dd}), directly independent from τ_c, c) contribution from inhomogeneous broadening (α_{hfc}) due to ^{1}H and other ^{14}N *hfc*, as mentioned above. Based on the data in Table 1 and expression (5), it is possible to evaluate the relative contribution of α/γ, β/γ, and δ/γ in ΔH_m. It was shown in [28] that in case of n equivalent nuclei combined with spin I, instead of $I(I+1)$ one should use $< I(I+1)>_m$, with an average $I(I+1)$ value for a given value of m. In case of $n = 2$, $I = 1$, $I_{eff} = 2$ and for $m = 2, 1, 0$, $<I(I+1)>_m$ is is respectively 6, 4, 8/3 in combination with $(\Delta A)^2/40$. For example, for any m, the calculated $\delta:\beta$ ratio is close to 1.5:1, which is in good correlation with the data obtained experimentally in this work for $\beta:\delta$, taking in mind that α cannot be evaluated correctly for PPDN, due to $\alpha_{hfc} \gg \alpha_1$ (the α_{hfc} data are presented later in this manuscript). The ratio $\delta:\beta$ obtained by (4) with Δg and ΔA (Table 1) is equal 1.5, while $\delta_1:\beta_1$ evaluated from spectra fitting (Fig. 3 a,b) is around 2–2.2. This result indicates a good correlation between experimental and theoretical data and gives rise to estimate the τ_c of the PPDN$^{-\bullet}$ rotation diffusion without spectrum fitting, using five linear independent equations of system (4), with ΔH_m in Gaussian settings for δ_1 and/or β_1 determination.

$$T_2^{-1} = \frac{1}{5\hbar^2}\left\{\begin{array}{l}\tau_C\left[\frac{4}{3}(\Delta g^2/3+\delta g^2)\mu_B^2H_0^2 + \frac{1}{8}(\Delta A^2+\delta A^2)(3I(I+1)+5m_I^2) - \frac{4}{3}(\Delta g\Delta A + 3\delta g\delta A)\mu_B H_0 m_I\right] + \\ \frac{\tau_C}{1+\omega^2\tau_C^2}\left[(\Delta g^2/3+\delta g^2)\mu_B^2H_0^2 + \frac{1}{8}(\Delta A^2+\delta A^2)(7I(I+1)-m_I^2) - (\Delta g\Delta A + 3\delta g\delta A)\mu_B H_0 m_I\right]\end{array}\right\} \quad (3)$$

$$\Delta H_{pp}(m) = \sqrt{2/\ln 2}\cdot(\alpha_0 + \alpha_1 + m\beta_1 + m^2\delta_1)\ ,\ m = 2,\ 1,\ 0,\ -1,\ -2 \quad (6a)$$

$$\beta_1 = \frac{\Delta H_{pp}(-1) - \Delta H_{pp}(1)}{2\sqrt{2/\ln 2}}\ or\ \beta_1 = \frac{\Delta H_{pp}(-2) - \Delta H_{pp}(2)}{4\sqrt{2/\ln 2}} \quad (6b)$$

$$\delta_1 = \frac{\Delta H_{pp}(2) - \Delta H_{pp}(1) + \beta_1}{3\sqrt{2/\ln 2}}\ or\ \delta_1 = \frac{\Delta H_{pp}(-2) - \Delta H_{pp}(-1) - \beta_1}{3\sqrt{2/\ln 2}} \quad (6c)$$

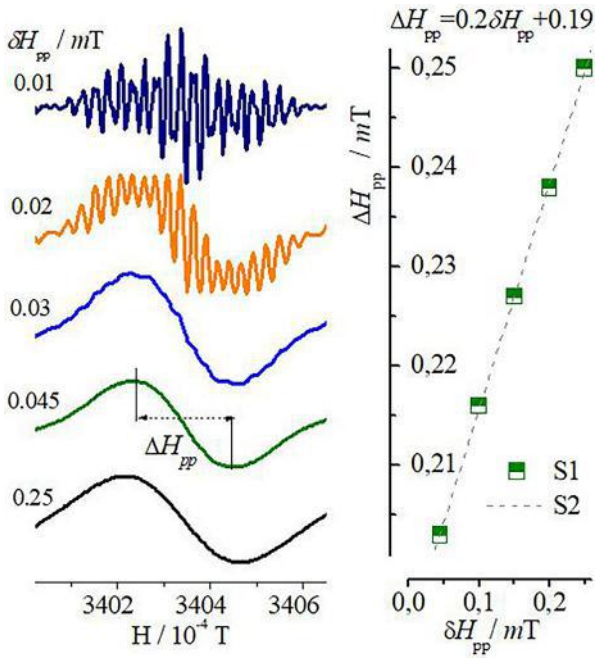

Fig. 6. a)the model PPDN$^{-\bullet}$ spectra, constructed with different δ_{pp}, using isotropic *hfc* constants of N(1,2), N(5,6), H(7,8), H(9,10), H(11,12), as listed in Table-I for the central line (m = 0 of the spectrum attributed to N(3,4)), b)$\Delta H_{pp} = F(\delta_{pp})$ of unresolved *hfc* spectrum.

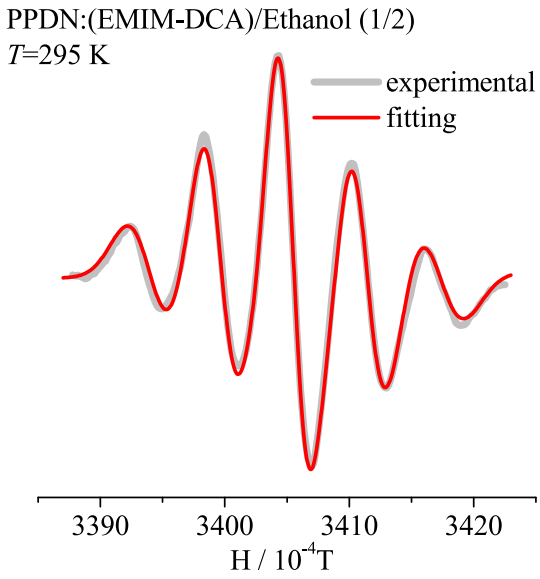

Fig. 7. PPDN$^{-\bullet}$ EPR spectrum recorded in binary blend EMIM-DCA/Ethanol in volume ratio (1/2).

Taking $\delta = 0.125(\Delta A)^2\gamma$ from (4) and $\Delta A \approx A_{//}$ from the spectrum in Fig. 3d one can evaluate τ_c by.

$$\tau_C = \frac{8\delta_1}{(\Delta A)^2\gamma} \tag{7}$$

where δ_1 is obtained from the system equations (6a) and solutions (6b,c). Assuming that $\delta_1 \approx k{\cdot}\beta_1$ in the applied temperature range and $1.52 < k < 2.2$ is the intermediate value between theoretical and experimental data, then, as mentioned above, only for the extreme *hfc* lines (m= ±2) of the PPDN$^{-\bullet}$ spectra, the expression (6) can be written as:

$$\tau_C = \frac{8k}{(\Delta A)^2\gamma}\left[\frac{\Delta H_{pp}(-2) - \Delta H_{pp}(2)}{4\sqrt{2/\ln 2}}\right] \tag{8}$$

In case of PPDN$^{-\bullet}$, without fitting the spectrum, the processing is suitable to the extreme spectral lines (m_I = ±2), namely half of ΔH_{pp} ($0.5{\cdot}\Delta H_{pp}$), as it is shown in Fig. 3b, that is utilized due to the minimum error attributed to the overlapping with the adjacent *hfc* lines (m=±1). The evaluation of τ_c by (6b) and (8) with $k \approx 2$ gives $\tau_c \approx 0.5$ *ns* (point ▲ in Fig. 5) and the result is close to that obtained by spectrum fitting $\tau_c \approx 0.47$ *ns*. The processing of the PPDN$^{-\bullet}$ spectra in RTIL had no obstacles from significant inhomogeneous broadening of the N(3,4) hyperfine lines due to unresolved *hfc* spectrum components that are assigned to two groups of two equivalent N(1,2; 5,6) and three groups of two equivalent H(7,8), H(9,10), H(11,12), as listed in Table 1. Inhomogeneous broadening is rather individual and depends from definite *hfc* parameters: as, for instance, the number of equivalent magnetic nuclear groups, even or odd number of nuclei in a group, and the actual *hfc* values. The model PPDN$^{-\bullet}$ spectra, constructed with isotropic *hfc* constants of N(1,2), N(5,6), H(7,8), H(9,10), H(11,12), are listed in Table 1. For the central line (m = 0) of N(3,4) the *hfc* spectra are introduced in Fig. 6a and they indicate the disappearance of the high resolution *hfc* structures in the EPR spectra with a set of effective individual linewidths at about $\delta H_m \geq 0.03$ mT. Therefore, the lower limit of the individual linewidth, hypothetically excluding other line broadening mechanisms, could be assigned to ~ 0.03 mT and the slope of the linear function in Fig. 6b gives α_{hfc} = 0.195 ± 0.005 mT. We note, that in case of PPDN$^{-\bullet}$, the inhomogeneous broadening α_{hfc}, as expected from the data introduced in the next paragraph, is increased by about one order of magnitude than α_{ex} and so the error deviation of α_0, obtained by the least-squares method fitting, is comparable with the α_{ex} values at the temperature range of effective exchange, namely $T > T_R$. Hence in PPDN$^{-\bullet}$ spectra processing, α_0 is set as a free parameter, the same in all *hfc* lines, and therefore it cannot be utilized as experimental data for the analysis of the residual linewidth in (4). However, the above explained approach certainly simplified the solution (6b-c) of the system of equations (6a) by hand. So far, we have checked the key details permitting the τ_c finding. Actually, the experimental temperature dependence of β_1, δ_1, obtained via PPDN:EMIM-DCA and PPDN:BMIM-BF4 spectra fitting, using ΔH_m(T) in form (4) demonstrates a correlation with the DSE theory of rotational relaxation (1).

Indeed, the E_η values that were obtained from the β_1, δ_1 dependencies versus temperature are in good agreement with literature data, as shown in Fig. 4a,b with accuracy at about several percent. Additionally, the calculated $\delta{:}\beta$ and experimental $\delta_1{:}\beta_1$ ratios are 1.52 and ~ 2.2 respectively, which indicates a good correlation of the experimental data with theory [28]. The τ_c data, obtained from δ_1 for PPDN$^{-\bullet}$ in both RTILs by (6b) are displayed in Fig. 5. The data corresponding to BMIM-BF4, are in focus here due to the possibility of the direct comparison of PPDN$^{-\bullet}$ $\tau_{c(P)}$ with $\tau_{c(TE)}$ of TEMPOL [17,18] in BMIM-BF_4. At the same temperatures in the range between 25 and 40 ^{0}C it was registered that $\tau_{c(P)}/\tau_{c(TE)} \approx 7$. Approaching spherical rotation, an evaluation of the hydrodynamic radius of PPDN and TEMPOL molecules, respectively R_P and R_{TE}, gives ratio $(R_P)/(R_{TE}) \approx 1.26$, i.e. $\tau_{c(PPDN)}/\tau_{c(TEMPOL)} \sim (1.26)^3 \approx 2$ (τ_c-$\sim R^3 \sim V$ (1a)), and thus, the "residual" ratio equals ≈7/2. Approximately, the same ratio was reported for TEMPOL and TEMPOL charged derivatives (TEcd) in [14,15] $\tau_{c(TEcd)}/\tau_{c(TE)} \approx 4$. Consequently, the PPDN$^{-\bullet}$ results confirm the data reported in [14], where it was concluded that the ionic interactions between the individual ions of the ILs and the ion radicals (ionic *sp*) diluted in ILs strongly influence the rotation of the ionic *sp* in ILs, while the neutral radicals do not as strong interact with IL as the RA.

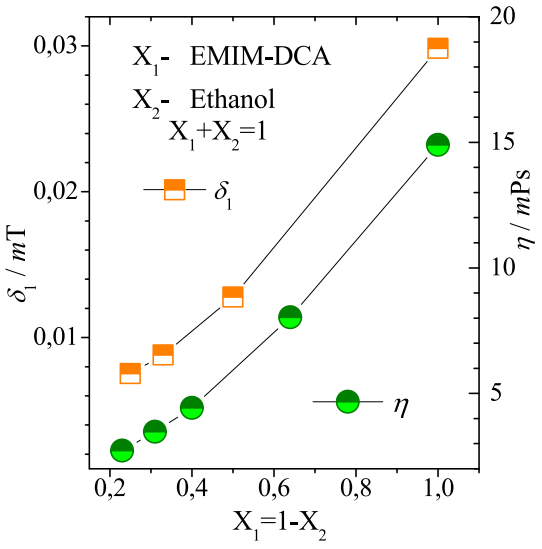

Fig. 8. Left axis: δ_1 dependence versus the relative part of EMIM-DCA volume in the binary blend EMIM-DCA/Ethanol. The right axis demonstrates the dynamic viscosity of the above blend (η -data are taken from reference [33]).

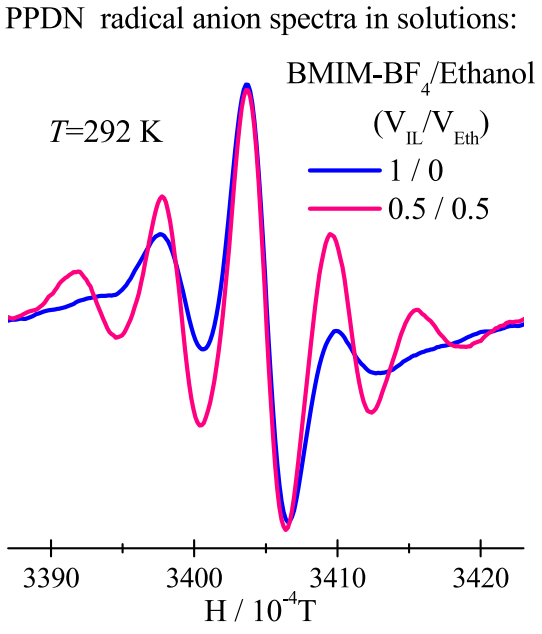

Fig. 9. The spectra were normalized to the maximum amplitude of the central line (m = 0): EPR spectra in ordinary BMIM-BF_4 and BMIM-BF_4/Ethanol with the equal parts of volume 0.5/0.5 respectively, recorded at T_R. Note, that **1** is attributed to the maximum volume of the solution in the in situ working area of the microwave cavity in both (1/0 and 0.5/0.5) solutions.

Additionally, the same tendency was registered by time-resolved fluorescence spectroscopy in perylene solution [32]. Our $PPDN^{-\bullet}$ data in BMIM-BF_4 (Fig. 5) at 313 K gives $\tau_{c(Per)} \approx 1.1$ *ns*, and for.

perylene in BMIM-BF_4 τ_c is around $\tau_{c(Per)} \approx 0.55$ *ns*, while their radiuses are nearly the same with a deviation of about 3–4%, which can be simply assed by energy minimization (geometric optimization) by MM2 force field calculation. The above ratio gives a hypothetical value for $V_{PPDN}/V_{peryl} = \tau_{c(P)} / \tau_{c(Per)} \approx 1.1$, i.e. ~ 10% difference, in contrast to the twice as high value of the experiment, that, at least qualitatively supports the above examples regarding

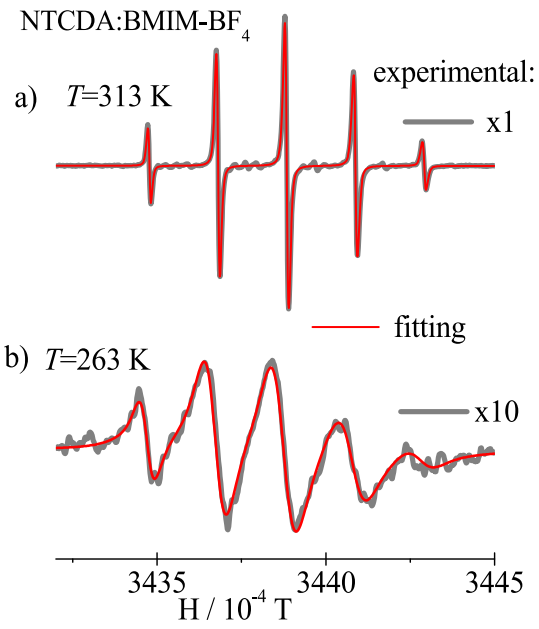

Fig. 10. NTCDA:BMIM-BF_4 EPR spectra recorded at a) T = 313 K and b) T = 263 K. $C = 4 \cdot 10^{-3}$mol/L.

nitroxides. One of the possible application of the $PPDN^{-\bullet}$ in RTILs study by EPR could be attributed to binary-systems of IL-IL, IL-(organic solvents) or IL-water [32–34]. An example of a spectrum recorded in the binary system EMIM-DCA:Ethanol (1:2) at 22 ^{0}C and the δ_1 dependence versus relative concentrations X_1 of EMIM-DCA in a binary blend with ethanol X_2 (X_1+X_2=1) are displayed respectively in Fig. 7 and Fig. 8. The data of δ_1=$F(X_1)$ are compared with the η data of EMIM-DCA:Ethanol binary blends, obtained at different relative concentrations of components [33] and the appropriate results are also displayed in Fig. 8. The correlation between δ_1 and the viscosity of the binary system, as shown in Fig.8, is evident and demonstrates the possibility of molecular diffusion study using $PPDN^{-\bullet}$ in binary blends including, at least, the RTILs, which were utilized in this work. Slopes of $\Delta\eta/\Delta X_1$ and $\Delta\delta_1/\Delta X_1$ of both functions in Fig. 8 predict the determination of η from δ_1 data with an accuracy of $\Delta\eta/\eta$ limited in case of $PPDN^{-\bullet}$ $\Delta\delta_1/\delta_1$ =7±1 % and the details of the numerical estimation are presented in SM-2d.

The analogic response of the *hfc* spectra to the η deviation in the blend is demonstrated in Fig. 9, where the $PPDN^{-\bullet}$ spectra in BMIM-BF_4 and BMIM-BF_4/Ethanol with the volume ratio 1/1 recorded at T_R are shown. BMIM-BF4:Ethanol EPR spectrum processing indicates that η of 1/1 blend at 22 ^{0}C coincidences with ordinary BMIM-BF4 η at 56 ^{0}C ± 1 °C, (Fig. 4 b), namely the viscosities ratio at these temperatures is ~ 6.5, that coincides with ~ 6.3 for the ordinary BMIM-BF4 and BMIM-BF4/Ethanol (1/1) mixture reported in [34]. As it was mentioned above, $PPDN^{-\bullet}$ is a relatively stable RA and in our experiments its life time under the CW light illumination is limited by the extreme values of ~ 40 min and ~ 250 min at room temperatures. The results of the kinetics depend on temperature, illumination power density, and therefore, in the case of a cylindrical sample, they are also sensitive to the position of the sample in a quartz tube of 2 mm in diameter relative to the emitter axis light beam (diameter 1.5 mm), i.e., to its deviation from the vertical (mirror) planes of symmetry. In accordance with the optimal geometry of illumination in a quartz cylinder, the axis of the light beam should pass as close as possible in this plane of symmetry. The lifetime of radicals also depends on the ratio of illuminated and possible dark zones of the sample,

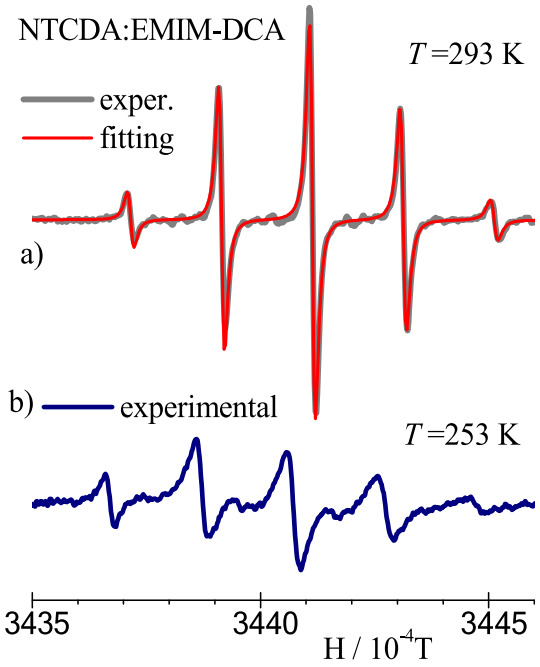

Fig. 11. NTCDA:EMIM-DCA EPR spectra recorded at a) T = 293 K and b) T = 253 K. C = 9·10^{-4}mol/L.

Table A1
NTCDA$^{-\bullet}$ ^{1}H *hfc* and g-tensors.

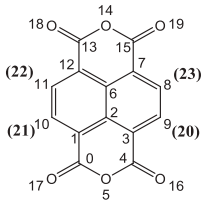

Atoms	*hfc* / *m*T	
	Exper.	DFT
$H_{(20,21,22,23)}$	**0.196**	**−0.182**
A_{iso}	–	**−0.23**
A_X	–	**−0.03**
A_Y	–	**−0.27**
A_Z	–	
g_x = **2.0022**, g_y = **2.0042**, g_z = **2.0042**, g_{iso} = **2.0032**		

Table A2
Parameters α (m=0), β, δ (/10^{-4} T)^2 calculated for X-band (PPDN$^{-\bullet}$, NTCDA$^{-\bullet}$) and K-band (NTCDA$^{-\bullet}$).

	α	β	δ
PPDN$^{-\bullet}$	X-band		
	55	21.7	33
NTCDA$^{-\bullet}$	X-band		
	4.7	1.2	0.9
	K-band		
	31	3.2	0.9

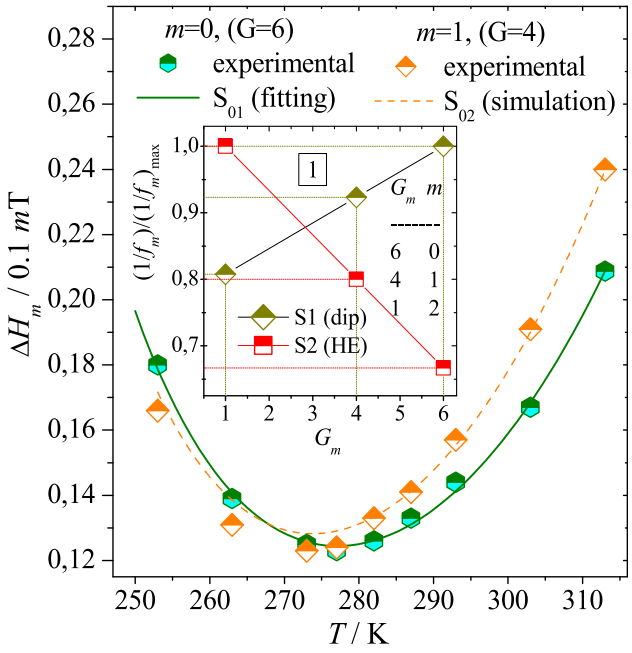

Fig. 12. $\Delta H_{(m)}$ temperature dependencies of EPR spectra in NTCDA$^{-\bullet}$: EMIM-DCA solution for m = 0 (G = 6), as well as the experimental and simulated data for m= ±1 (G = 4). In insert **1,** the normalized values of $1/f_m$ dip-dip and HE interactions versus G_m are shown.

and the presence of the latter can increase the lifetime. The second reason of an upper limit should be assigned to the rate of a diamagnetic product formation under the CW Xe-lamp excitation, but at this stage, the chemical and other analytical methods of product analysis has not been carried out. However the supposition, regarding the kinetics model of PPDN$^{-\bullet}$ formation/annihilation reaction steps with appropriate experimental data, obtained at different temperatures is exhibited in SM-2c.

5. NTCDA

Electrolytically generated radical anion of naphthalene-l,4,5,8-tetracarboxylic acid derivatives, including 1,4,5,8-Naphthalenete tracarboxylic dianhydride (NTCDA$^{-\bullet}$) are well known and were firstly detected by EPR a long time ago [36]. However, we could not find the data regarding light-induced NTCDA$^{-\bullet}$ registration in liquid solutions and ILs by EPR in literature. Only four equivalent hydrogen atoms in NTCDA$^{-\bullet}$ (Table A1) are responsible for the EPR hyperfine structure, and this greatly facilitates the data processing procedure. Experimental and by DFT calculated g- and ^{1}H *hfc*- tensor components of NTCDA$^{-\bullet}$ as well α, β, δ evaluated for both radicals in X-band and additionally NTCDA$^{-\bullet}$ in K-band are introduced respectively in Tables A1 and A2.

Note, that the *hfc* anisotropy in NTCDA$^{-\bullet}$ is considerably lower than in PPDN$^{-\bullet}$, hence in case of NTCDA$^{-\bullet}$ $\delta g = (g_x\text{-}g_y)/2$, $\delta A = (A_x\text{-}A_y)/2$ are comparable with Δg, ΔA and are not omitted in (3), consequently, calculated α, β, δ displayed in Table A2 are expressed by.

$$\alpha = \frac{4}{45}(\Delta g H_0)^2 + \frac{4}{15}(\delta g H_0)^2 + \frac{3}{40}\Delta A^2 I(I+1)\ ,\ \beta = \frac{4}{5}\left[\frac{1}{3}\Delta A \Delta g H_0 + \delta A \delta g H_0\right],\ \delta = \frac{1}{8}\Delta A^2 + \frac{2}{3}\delta A^2 \quad (8)$$

The X-band data in Table A2 indicate the essential difference between α, β, δ of both anion radicals due to the difference in the A_i -tensor magnitudes and therefore the *hfc* anisotropy. The experimental and handled EPR NTCDA$^{-\bullet}$ spectra confirm the weak contribution of the rotational diffusion to ΔH_m broadening at the low viscosity region and examples of NTCDA$^{-\bullet}$ spectra in BMIM-BF4 at 313 K and EMIM-DCA at 293 K are shown respectively in Fig. 10 and Fig. 11a. Vice versa, at low temperatures (high viscose RTILs range), the contribution to the *hfc* linewidth, which is assigned to the NTCDA$^{-\bullet}$ rotational diffusion, increases. That was detected by the spectra introduced in Fig. 10b and Fig. 11b, where the difference of ΔH_m of the extreme m=±2 hyperfine lines is visually detectable, but the processing of the spectra recorded at $T > T_R$ shows the limitation that is connected with the insignificant α, β, δ values. However, an inessential anisotropy of NTCDA$^{-\bullet}$ *hfc*-tensors

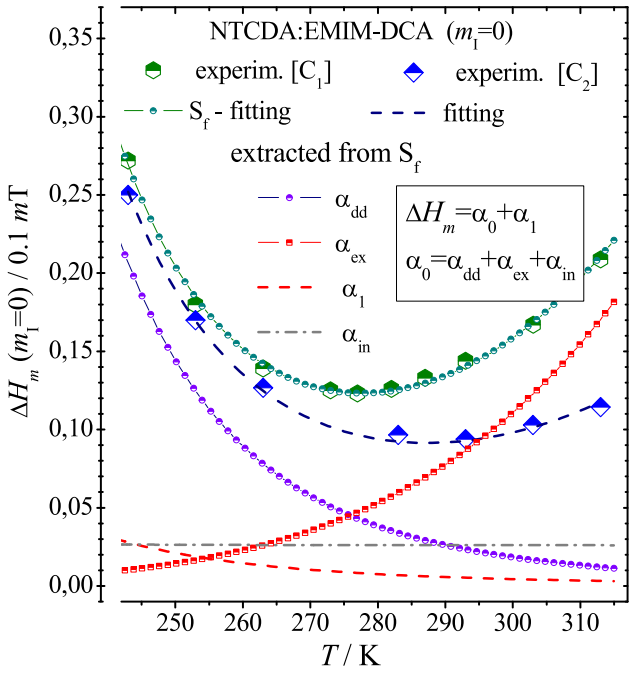

Fig. 13. $\Delta H_{(m=0)}$ temperature dependency of NTCDA$^{-\bullet}$ EPR spectra in EMIM-DCA solutions with two concentrations of NTCDA$^{-\bullet}$: $C_1 = 3{\cdot}10^{-3}$ and $C_2 = 9{\cdot}10^{-4}$ mol/L. The appropriate denominations of experimental, fitted and extracted curves, assigned to the different mechanisms, are displayed in inserts of Fig.13 and SM-3.

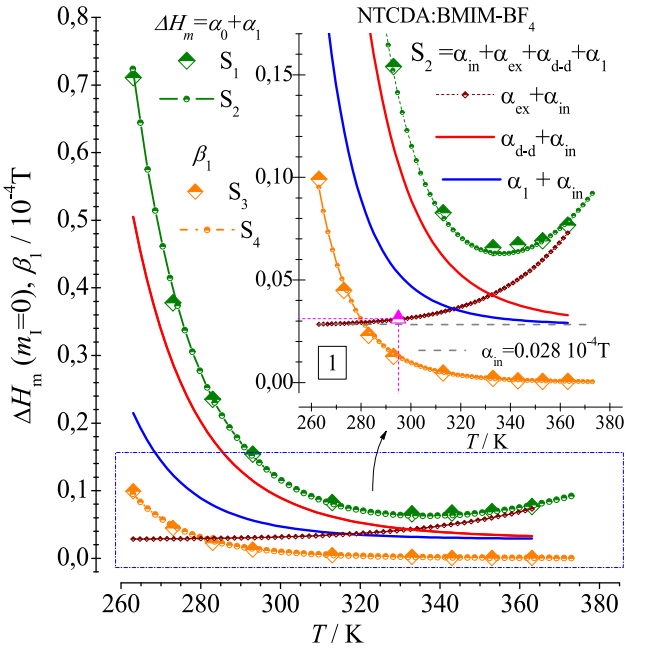

Fig. 14. $\Delta H_{(m=0)}$ temperature dependency of NTCDA$^{-\bullet}$ EPR spectra in BMIM-BF_4 solutions with concentrations of NTCDA$^{-\bullet}$ $C_1 \approx 6.5{\cdot}10^{-4}$ mol/L (E_η = 4600 K, E_t = 4350 K). The denominations of experimental, fitted and extracted curves, assigned to the different mechanisms, are displayed in inserts. S_1-ΔH_m experimental, S_2 –fitting, S_3- β_1 experimental, S_4- β_1 fitting.

ΔA = 0.137 mT, in comparison with the typical nitroxides ΔA = 2.78 mT (more details are in SM-3c) as well as the absence of inhomogeneous broadening mentioned before, gives rise of sure Heisenberg spin exchange (HE) detection. This could be useful for the study of ion radical reaction kinetics, those are limited by the diffusion, especially the evaluation of translational diffusion and the rate constant k_2 of NTCDA$^{-\bullet}$ collisions that are resulting in an electron spin exchange. Note, that contrary to PPDN$^{-\bullet}$ in case of NTCDA$^{-\bullet}$, the parameters α_0 and α_1 are in focus instead of the β_1, δ_1 ones (5).

Taking into account the above data of NTCDA$^{-\bullet}$ EPR parameters anisotropy in comparison with nitroxides (SM-3c), one can expect more sensitivity of α_0 to the concentration-dependent mechanisms of EPR line broadening like HE and dipolar spin coupling due to the absence of α_{hfc} as mentioned above. Examples of NTCDA$^{-\bullet}$ spectra fitting are shown in Fig. 10 and Fig. 11. In further analysis of the ΔH_m broadening mechanism, we have followed an approach, which was reported in [37–38]. The effective line width $1/T_2^*$ in the case of spin exchange in general is expressed as

$$\frac{1}{T_2^*} = \frac{1}{T_2(0)} + \frac{1}{\tau_2} P \tag{9a}$$

$$\frac{1}{\tau_2} = \left(\frac{\sqrt{3}}{2}\right) f_m \, \gamma_e \delta_{ex(m)} = k_2 C = k_{ex} C, P = \frac{J_0^2 \tau_1^2}{1 + J_0^2 \tau_1^2} \tag{9b}$$

Where $1/T_2(0)$ is the relaxation rate that corresponds to other relaxation mechanisms independent of the exchange, τ_2 is the mean time between bimolecular collisions, τ_1 is the mean lifetime of a radical pair, J_0 is the contact value of the exchange integral $J(r)$, which corresponds to the exchange interactions of the $\mathbf{S}_1$ and $\mathbf{S}_2$ spins than can be described by the Hamiltonian $J(r)\mathbf{S}_1\mathbf{S}_2$, k_{ex} is the rate constant of the bimolecular spin HE, C is the radical concentration, γ_e is the electron gyromagnetic ratio, $\delta_{ex(m)} = \delta_{ex(m)}(C) - \delta(c_0)$ is assigned to the excess line broadening, depending on radical concentration, where c_0 is a concentration corresponding to $\delta_{ex(m)}(c_0) \approx 0$ and $\delta(c_0)$ is the width independent of concentration. In RTILs, the last set mainly relates to $c_0 \leq 10^{-4}$ mol/L. In expression (9b), f_m is a statistical factor, which denotes the fraction of all resonant hyperfine transitions m, associated with exchange, including degenerated ones (if there are any), namely.

$$f_m = \frac{N}{N - 2G_m}, \; N = \sum_m G_m \tag{10}$$

where N is the total number of electron-nuclear spin eigenstates and G_m denotes the degeneracy of the m-th *hfc* line of ESR spectrum. Therefore, the NTCDA$^{-\bullet}$ spectra fitting has been carried out with the set of individual parameters α_0 depended on m, i.e. in (4) $\alpha_0(m)$ is: $\alpha_0(0)$, $\alpha_0(1) = \alpha_0(-1)$, $\alpha_0(2) = \alpha_0(-2)$. However, the concentration-dependent line broadening can also arise from dipole-dipole interactions between the electron spins on neighboring radicals ($\delta_{d(m)}$) [37]. The appropriate data of the contribution of both mechanisms is discussed elsewhere [37,38]. There, it was highlighted, that the excess linewidth, assigned to the sum of HE and dipolar contributions ($\delta_m = \delta_{ex(m)} + \delta_{d(m)}$), is given by the sum of two terms that, respectively, depend directly ($\sim D_t$) and inversely ($\sim 1/D_t$) on the translational diffusion coefficient D_t. Assuming an Arrhenius mechanism of reaction, $D_t = D_0{\cdot}\exp(-E_t'/T)$, where E_t' is the activation energy of translational diffusion in K unit, then the excess linewidth δ_m can be written as.

$$\begin{aligned}\delta_m(C) &= \delta_m(C + c_0) - \delta(c_0) \\ &= [A_1 \exp(-E_t'/T) + B_1 \exp(E_t'/T)]C\end{aligned} \tag{11}$$

where $A_1 = P_1(d{\cdot}D_0)$, $B_1 = P_2(d{\cdot}D_0)^{-1}$, $d = 2R$ is the encounter distance for two radicals undergoing exchange and P_1, P_2 are parameters depending on C, f_m, S as well as $\hbar$, γ_e and Avogadro's number N_0 [37]. Contrary to the most of nitroxide radicals (I = 1), G_m = 1 for all m = 1, 0, −1, in NTCDA$^{-\bullet}$, G = 1, 4, 6 are attributed to the *hfc* lines assigned respectively to m= ±2, ±1, 0, and the difference between $\delta_m \sim 1/(\tau_2 f_m)$ in case of slow strong exchange, especially $(J_0\tau_1)^2 \gg 1$ (9b) could be reliably detected experimentally. In general,

the comparison of $\alpha_0(m)$ values is expedient by a complete processing of ΔH_m temperature dependence in form (5). The low temperature experiments ($T < T_R$) demonstrate the obvious contribution of rotational diffusion (spectra in Fig. 10b and Fig. 11b) due to the width difference of the *hfc* lines that are assigned to ± *m*. The experimental *hfc* spectra have been fitted with the usual set of relative *hfc* line amplitudes 1:4:6:4:1 for four equivalents ^{1}H with above.

$$\Delta H_{(m)} == \alpha_0 + \alpha_1 + m\beta_1 + m^2\delta_1 \quad (12)$$

where $\alpha_0 = \alpha_{ex} + \alpha_{dd} + \alpha_{in} = [A_1\exp(-E_t'/T) + B_1\exp(E_t'/T)]C + \alpha_{in}$. To minimize an influence of rotational diffusion contribution, i.e. exclusion of β_1 and δ_1 in HE data processing, $\Delta H_{(m)}$ dependence versus T has been considered for the central *hfc* line ($m = 0$). It is expected, that the contribution of α_1 in the range of effective HE at $T > T_R$ should be minimal ($\alpha_1 \ll \alpha_{ex}$) due to τ_c decreasing with exponential increasing T (1 a,b). However, in spite of preference, regarding the translational diffusion study in NTCDA solutions, here, it should be highlighted that in BMIM-BF$_4$ solution τ_c exceeds several times its value in EMIM-DCA. The dependence $\beta_1 \sim F(T)$ could be evaluated experimentally for the determination of E_η (like in case of PPDN$^{-\bullet}$), assuming, that the parameter β_1 is not even indirectly dependent from an exchange mechanism. In a model setting in (9–11) the correlation between the model and the experimental α_0 that is attributed to the different m, namely, f_m ($\delta_m \sim 1/f_m$,) should be checked in the first place. The experimental and fitted temperature dependencies of $\Delta H_{(m)}$ in NTCDA$^{-\bullet}$:EMIM-DCA solution for $m = 0$ ($G = 6$), as well as experimental and simulated for $m = \pm1$ ($G = 4$), are shown in Fig. 12. The result demonstrates a good correlation of experimental data with calculated in the observed temperature interval, corresponding to the dominating HE in this solution, in particular for $T > 280$ K. Indeed, S_{02} is constructed from parameters, obtained by central line fitting (S_{01}) with an appropriate difference of $1/f_m$ values, calculated by (10). For instance for HE $(1/f_{\pm1})/(1/f_0) = (3/4)/(5/8) = 6/5$, which coincides with the experimental data introduced in Fig. 12 in a temperature range of dominating HE, as mentioned above. In insert **1** in Fig. 12, the on the maximum normalized values of $1/f_m$ dipole–dipole and HE interactions versus G_m are shown (note, $\delta_{d(m)} \sim 1/f_{m(-d)} \sim (5\ N + 8G_m)/24\ N$ [37]). The resulting $\Delta H_{(m)}$ temperature dependence of NTCDA$^{-\bullet}$ in EMIM-DCA and BMIM-BF$_4$ solutions are shown in Fig. 13 and Fig. 14, respectively, where the contributions of dipolar and HE are separated. This enables to evaluate the translational diffusion parameters utilizing the $\alpha_{ex} = F(T)$ dependency. The additional consideration with: a) the details of the sets in $\Delta H_{(m)}$ for the least-squares analysis, b) an α_{in} estimation based on $\alpha_0 = F(C)$ dependency, c) α_{ex} and α_{dd} versus T for the solution with $C_2 = 9{\cdot}10^{-4}$ mol/L, d) appropriate numerical parameter values are introduced in the SM-3 paragraph. According to BMIM-BF$_4$ solution, the fitting of the $\beta_1 \sim F(T)$ experimental data, displayed in Fig. 13 surely confirms the dependency $\beta_1 \sim \tau_c \sim (1/T){\cdot}exp(E_\eta/T)$ with $E_\eta \approx 4500$ K, which is close to that obtained in PPDN$^{-\bullet}$:BMIM-BF$_4$ (see Fig. 4b) with a deviation of about 8 %. The exchange rate constant is evaluated from (9b), utilizing α_{ex} data presented in Fig. 13 and Fig. 14.

$$k_{ex} = \left(\frac{\sqrt{3}}{2}\right)\frac{f_m\ \gamma_e\alpha_{ex}}{C} \quad (13)$$

At T≈ 295 K, for EMIM-DCA (Fig. 13, $\alpha_{ex} \approx 0.009{\cdot}$ mT, $C \approx 2.6{\cdot}10^{-3}$ mol/L), $k_{ex} \approx 8{\cdot}10^8$ *L*/sec·mol and in BMIM-BF$_4$ (Fig. 14, $\alpha_{ex} = S_{2C} - \alpha_{in} \approx 4{\cdot}10^{-4}$ mT which is denominated as Δ in insert **1**, $C \approx 0.65{\cdot}10^{-3}$ mol/*L*), $k_{ex} \approx 0.68{\cdot}10^8$ L/s·mol. The above results correlate with the analog of TEMPOL in BMIM-BF$_4$. Indeed, k_{ex} of the hypothetical "neutral NTCDA radical" should be bit higher (5–10%) than in TEMPOL (≈10^8 L/s·mol [18]), due to the proportionate difference in the diameters. However, the solvation is a consequence of the complex interplay of the H-bonding (R-O----H) [15] especially in case of NTCDA$^{-\bullet}$ and as well as Coulomb interactions between RA should decrease the rate of exchange. This result confirms the supposition that translational diffusion of the ion radicals is also sensitive to electrostatic interactions [37,38] as it was mentioned above for the rotational molecular motions [14,15]. An evaluation of D_t, in BMIM-BF$_4$ was carried out using an expression for Brownian diffusion [37,39].

$$\frac{1}{\tau_2} = \left(\frac{\sqrt{3}}{2}\right)f_m\ \gamma_e\alpha_{ex} = 4\pi dD_tC_N \quad (14)$$

where C_N is the number density of radicals, related to the molar concentration C of the solution with $C_N = 10^{-3}N_AC$, where N_A is the Avogadro number. Utilizing $f_m = 8/5$ ($m = 0$), the NTCDA diameter $d \approx 8{\cdot}10^{-8}$ cm, $\alpha_{ex} \approx 0.0005$ mT at $T = 295$ K and $C \approx 7{\cdot}10^{-4}$ mol/L, it is possible to obtain $Dt \approx 2.1{\cdot}10^{-4}$ cm^2/s, i.e. less than that of TEMPOL in BMIM-BF4, namely $Dt \approx 3{\cdot}10^{-3}$ cm^2/s at $T = 295$ K [18], which indirectly confirms the effect of hydrogen bonds H···O and Coulomb interactions on the diffusion of NTCDA$^{-\bullet}$.

NTCDA data $D_t = F(T)$ in EMIM-DCA and BMIM-BF4 solutions presented in Fig. S11 (SM-3d) were estimated by (14) using the results of α_{ex} shown in Fig. 13 and Fig. 14. Additionally, returning back to the Table A2, point out that α_1, β_1 are dependent from external magnetic field strength ***H*** and the comparison of the experimental α_1, β_1, δ_1 and calculated α, β, δ with the same data, obtained by higher microwave frequency is the important procedure to justify the model choice. The above has been carried out utilizing K-band EPR technique. In this case, one can expect at about $[H_{0K}/H_{0X}]^2 = [0.864\ T/0.344\ T]^2 \approx 6.3$ times higher α_1 in K-band than in X-band. That is confirmed by the NTCDA$^{-\bullet}$ spectra processing in BMIM-BF4 solution, recorded using X-band (Fig. 10a) and using K-band (Fig. 15) at T_R. Actually, the experimental $\alpha_1 \approx 0.022$ mT and $\alpha_1 = 0.0034$ mT, obtained respectively by K- and X-bands, give $0.22/0.034 \approx 6.5$, which coincidences well with the same ratio for α, calculated by (5): $31/4.7 \approx 6.6$ (compare the insert in table A, Fig. 15). This result is confirmed by the same

Table B

EPR	α	(α_1)	β	(β_1)
K-	31	(0.22)	3.2	(0.02)
X-	4.7	(0.03)	1.2	(0.01)

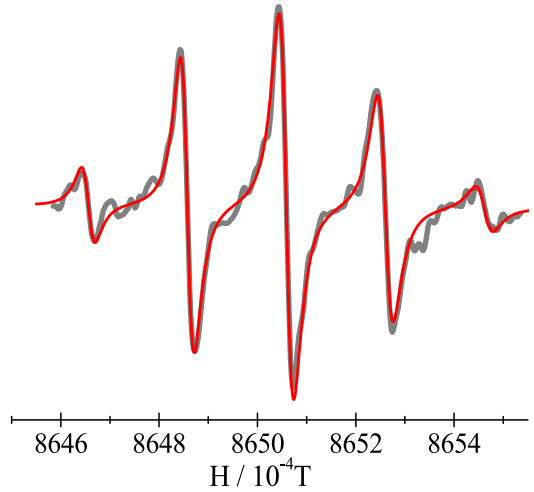

Fig. 15. K-band EPR spectrum of NTCDA$^{-\bullet}$:BMIM-BF4 solution obtained with the following experimental sets: C = $3{\cdot}10^{-4}$ mol/L, $P_{\mu w}$ = 0.3 mW, H_{mod} = 0.01 mT, T = 294 K, λ = 532 nm. The insert "Table-B" shows α, β calculated by (4), (8), as well as experimentally obtained α_1, β_1 for the X- and K-bands.

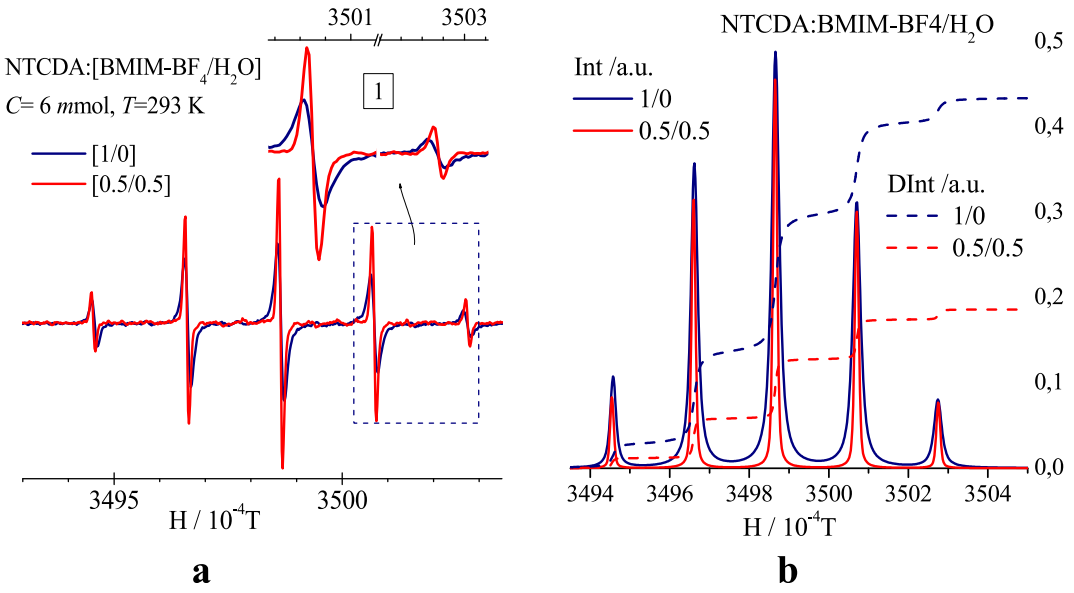

Fig. 16. a) Light induced NTCDA$^{-\bullet}$ ESR spectra recorded in BMIM-BF_4 and BMIM-BF_4/H_2O with the volume ratio ~ 0.5/0.5. Note, that 0.5 + 0.5 = 1 is assigned to the same volume of samples in both solutions. The ratio 1/0 corresponds to the ordinary BMIM-BF_4 solution. b) constructed integral and double integral depiction of the experimental data.

experimental ratio of α_1 and β_1 (Table A in the insert in Fig. 15) $\alpha_{1(K\text{-}b)}/\alpha_{1(X\text{-}b)} \approx 0.22/0.032 \approx 6.8$ and the ratio for β and β_1 are respectively $\beta_{(K\text{-}b)}/\beta_{(X\text{-}b)} \approx 3.2/1.2 \approx 2.66$ and $\beta_{1(K\text{-}b)}/\beta_{1(X\text{-}b)} \approx 0.022/0.01 \approx 2.2$.

The spectrum in Fig. 15 refers to the solution with a radical concentration of < $3{\cdot}10^{-4}$ mol/L, and therefore the HE contribution can be neglected. An NTCDA$^{-\bullet}$ application for binary IL/H2O blends [40] study as a spin probe for EPR is confirmed by the simple comparison of NTCDA:BMIM-BF_4/H_2O (1/1 v.r.) and ordinary NTCDA: BMIM-BF_4 EPR spectra presented in Fig. 16a. The effective linewidth ($\alpha_1 + \alpha_0$) of the binary blend responds sufficiently to decreasing of solution viscosity, due to low η of water, as well as the RA concentration reduction in mixture, that leads to a reduction of ($\alpha_{dd} + \alpha_1 + \alpha_{in}$) to a minimum of ~ 0.0055 mT, which is limited only by $\alpha_{in} \approx 0.003$ mT with an accuracy of about ± 0.0005 mT. Note, that in BMIM-BF4 $\alpha_{ex} \ll \alpha_{dd}$ at $T < T_R$, which is reflected in Fig. 14. Constructed from experimental spectra integral (Int) and double integral (DInt), the data displayed in Fig. 16b visually demonstrate the results of spectra processing, in particular a remarkable reduction to around half the EPR linewidth and DInt. The above example demonstrates the availability of aqueous binary blends analysis by NTCDA$^{-\bullet}$ EPR, firstly by the optimization of blended components ratio in order to study the translational diffusion by the *T*- and *C*-dependent exchange.

Note that at the ratio IL/$H_2O \approx 1/1$ (0.5/0.5) the α_1 contribution practically disappears even at room temperature. However, the detailed consideration of this task, including EMIM-DCA/H_2O binary blend, is beyond the scope of this work.

6. Conclusion

In this study, the suppositions and conclusions concerning radical products of light induced reactions, initiated by the electron transfer from an anion of an IL, based on EPR and DFT data, are discussed. The formation of anion radicals from the potential electron acceptors PPDN and NTCDA in EMIM-DCA and BMIM-BF_4 RTIL solutions under relatively weak steady state UV and visible light illumination with power densities around several ten mW/cm^2, has been detected using the EPR method. The experimental spectra of NTCDA$^{-\bullet}$ and PPDN$^{-\bullet}$ are in good agreement with the calculated ones obtained by DFT. It was found that the lifetime of the NTCDA$^{-\bullet}$ in BMIM-BF_4 exceeds the ones in EMIM-DCA as well as the life time of PPDN$^{-\bullet}$ in both above mentioned ILs by several times. With regards to the main goal of this study, an investigation of NTCDA$^{-\bullet}$ and PPDN$^{-\bullet}$ as new spin probes for rotational and translational motion study in the above pure ILs and tentative in their blends with some other organic liquids as well water has been carried out. It was found that PPDN$^{-\bullet}$ is rather less suitable for a detailed intermolecular spin exchange analysis, due to the strong contribution of the inhomogeneous *hfc* line broadening. However, it is well suited to study the rotational diffusion, due to the strong *hfc* anisotropy in comparison with NTCDA$^{-\bullet}$, while the last is an excellent probe for translational diffusion controlled process investigations in these IL solutions. NTCDA$^{-\bullet}$ can be generated in EMIM-DCA-water and BMIM-BF_4-water blends under visible light (532 nm) excitation, which leads to the formation of active short living IL anion radicals in water containing blends, which are of potential interest for studies on biological systems. However, in this case the active radicals are generated through the absorbed photon energy ($\lambda \sim 532$ nm), which is far beyond the range of the energy required for degrading water ($\lambda \sim 180$ nm), and which results in the formation of highly oxidizing OH$^\bullet$ and H$^\bullet$ radicals that pose a serious risk to most biomolecular systems. The EPR investigations of light induced radical anions in binary liquids demonstrate that PPDN and NTCDA could be utilized to study the translational and rotational diffusion in binary and heterogeneous composed liquid systems, including IL-IL, IL-organic solvents, IL-water, as well as their combinations.

Declaration of Competing Interest

The authors declare that they have no known competing financial interests or personal relationships that could have appeared to influence the work reported in this paper.

Acknowledgments

We thank Torsten Saendig, and Dr. Arne Albrecht for helping with the realization of scheme for the optical pumping in K-band

EPR experiments. This work was supported by the subsidy allocated to Kazan Federal University for the state assignment in the sphere of scientific activities (No 0671-2020-0051). VIK is grateful to partial RFBR support (Grant No 18-29-20011-mk) of some experiments in the IPCH RAS according to the State Assignment, No AAAA-A19-119032690060-9

Appendix A

See Table A1 and Table A2.

Appendix B. Supplementary material

Supplementary data to this article can be found online at https://doi.org/10.1016/j.molliq.2022.119631.

References

[1] K. Dong, X. Liu, H. Dong, X. Zhang, S. Zhang, Multiscale Studies on Ionic Liquids, Chem. Rev. 117 (2017) 6636–6695, https://doi.org/10.1021/acs.chemrev.6b00776.
[2] N.V. Plechkova, K.R. Seddon, Applications of ionic liquids in the chemical industry, Chem. Soc. Rev. 37 (2008) 123–150, https://doi.org/10.1039/B006677J.
[3] M.J. Earle, K.R. Seddon, Ionic liquids. Green solvents for the future, Pure Appl. Chem. 72 (2000) 1391–1398, https://doi.org/10.1351/pac200072071391.
[4] S. Ravula, N.E. Larm, M.A. Mottaleb, M.P. Heitz, G.A. Baker, Vapor pressure mapping of ionic liquids and low-volatility fluids using graded isothermal thermogravimetric analysis, ChemEngineering. 42 (2019) 1–12, https://doi.org/10.3390/chemengineering3020042.
[5] E.M. Siedlecka, M. Czerwicka, S. Stolte, P. Stepnowski, Stability of ionic liquids in application conditions, Curr. Org. Chem. 15 (2011) 1974–1991, https://doi.org/10.2174/138527211795703630.
[6] K.S. Egorova, E.G. Gordeev, V.P. Ananikov, Biological activity of ionic liquids and their application in pharmaceutics and medicine, Chem. Rev. 117 (2017) 7132–7189, https://doi.org/10.1021/acs.chemrev.6b00562.
[7] Y. Cao, T. Mu, Comprehensive investigation on the thermal stability of 66 ionic liquids by thermogravimetric analysis, Ind. Eng. Chem. Res. 53 (2014) 8651–8664, https://doi.org/10.1021/ie5009597.
[8] I. Shkrob, T. Marin, J. Wishart, Radiation Induced Reactions and Fragmentation in Room Temperature Ionic Liquids, in: A. Lund, M. Shiotani (Eds.), Applications of EPR in Radiation Research, Springer, Cham, 2014, pp. 453–485, https://doi.org/10.1007/978-3-319-09216-4_12.
[9] T. Konishi, Y. Sasaki, M. Fujitsuka, Y. Toba, H. Moriyama, O. Itoa, Persistent C60 anion-radical formation via photoinduced electron transfer from tetraphenylborate and triphenylbutylborate, J. Chem. Soc., Perkin Trans. 2 (1999) 551–556, https://doi.org/10.1039/A808120D.
[10] A. Aster, E. Vauthey, More than a solvent: donor–acceptor complexes of ionic liquids and electron acceptors, J. Phys. Chem. B 122 (2018) 2646–2654, https://doi.org/10.1021/acs.jpcb.8b00468.
[11] A. Kawai, T. Hidemori, K. Shibuya, Polarity of room-temperature ionic liquid as examined by EPR spectroscopy, Chem. Lett. 33 (2004) 1464–1465, https://doi.org/10.1246/cl.2004.1464.
[12] R.G. Evans, A.J. Wain, C. Hardacre, R.G. Compton, An electrochemical and ESR spectroscopic study on the molecular dynamics of TEMPO in room temperature ionic liquid solvents, ChemPhysChem 6 (2005) 1035–1039, https://doi.org/10.1002/cphc.200500157.
[13] V. Strehmel, A. Laschewsky, R. Stoesser, A. Zehl, W. Herrman, Mobility of spin probes in ionic liquids, J. Phys. Org. Chem. 19 (2006) 318–325, https://doi.org/10.1002/poc.1072.
[14] R. Stoesser, W. Herrmann, A. Zehl, V. Strehmel, A. Laschewsky, ESR spin probes in ionic liquids, ChemPhysChem 7 (5) (2006) 1106–1111, https://doi.org/10.1002/cphc.200500651, In this issue.
[15] V. Strehmel, H. Rexhausen, P. Strauch, Influence of imidazolium bis (trifluoromethylsu lfonylimide) s on the rotation of spin probes comprising ionic and hydrogen bonding groups, Phys. Chem. Chem. Phys. 12 (2010) 1933–1940, https://doi.org/10.1039/B920586A.
[16] Y. Akdogan, J. Heller, H. Zimmermann, D. Hinderberger, The solvation of nitroxide radicals in ionic liquids studied by high-field EPR spectroscopy, Phys. Chem. Chem. Phys. 12 (2010) 7874–7882, https://doi.org/10.1039/C001602K.
[17] B.Y. Mladenova, D.R. Kattnig, G. Grampp, Room-temperature ionic liquids discerned via nitroxyl spin probe dynamics, J. Phys. Chem. B 115 (2011) 8183–8198, https://doi.org/10.1021/jp201703c.
[18] B.Y. Mladenova, N.A. Chumakova, V.I. Pergushov, A.I. Kokorin, G. Grampp, D.R. Kattnig, Rotational and translational diffusion of spin probes in room-temperature ionic liquids, J. Phys. Chem. B 116 (2012) 12295–12305, https://doi.org/10.1021/jp306583g.
[19] Strehmel, Radicals in ionic liquids, ChemPhysChem 13 (2012) 1649–1663, https://doi.org/10.1002/cphc.201100982.
[20] V. Strehmel, S. Berdzinski, H. Rexhausen, Interactions between ionic liquids and radicals, J. Mol. Liq. 192 (2014) 153–170, https://doi.org/10.1016/j.molliq.2013.12.007.
[21] Y. Miyake, A. Kawai, Solvation and rotational diffusion of solutes in room temperature ionic liquids as studied by EPR spectroscopy with nitroxide spin probing method, Appl. Magn. Reson 49 (2018) 825–835, https://doi.org/10.1007/s00723-018-1025-y.
[22] D. Merunka, M. Peric, Measuring radical diffusion in viscous liquids by electron paramagnetic resonance, J. Mol. Liq. 277 (2019) 886–894, https://doi.org/10.1016/j.molliq.2019.01.006.
[23] B.Y.M. Kattnig, N.A. Chumakova, D.R. Kattnig, I.A. Grigor'ev, G. Grampp, A.I. Kokorin, Influence of the electric charge of spin probes on their diffusion in room-temperature ionic liquids, J. Phys. Chem. B 125 125 (32) (2021) 9235–9243, https://doi.org/10.1021/acs.jpcb.1c02493, In this issue.
[24] J.R. Millgan, J.A. Agulilera, R.A. Paglinawan, J.F. Ward, Mechanism of DNA damage by thiocyanate radicals, Int. J. Radiat. Biol. 76 (10) (2000) 1305–1314, https://doi.org/10.1080/09553000050151574.
[25] T.G. St Denis, D. Vecchio, A. Zadlo, A. Rineh, M. Sadasivam, P. Avci, L. Huang, A. Kozinska, R. Chandran, T. Sarna, M.R. Hamblin, Thiocyanate potentiates antimicrobial photodynamic therapy: In situ generation of the sulfur trioxide radical anion by singlet oxygen, *Free Radic*, Biol. Med. 65 (2013) 800–810, https://doi.org/10.1016/j.freeradbiomed.2013.08.162.
[26] A.K. Vijh, B.E. Conway, Electrode kinetic aspects of the Kolbe reaction, Chem. Rev. 67 (1967) 623–664, https://doi.org/10.1021/cr60250a003.
[27] L. Das, R. Kumar, D.K. Maity, S. Adhikari, S.B. Dhiman, J.F. Wishart, Pulse radiolysis and computational studies on a pyrrolidinium dicyanamide ionic liquid: Detection of the dimer radical anion, J. Phys. Chem. A 122 (2018) 3148–3155, https://doi.org/10.1021/acs.jpca.8b00978.
[28] D. Kivelson, Theory of ESR Linewidths of Free Radicals, J. Chem. Phys. 33 (1960) 1094–1106, https://doi.org/10.1063/1.1731340.
[29] R. Wilson, D. Kivelson, ESR Linewidths in Solution. I. Experiments on Anisotropic and Spin-Rotational Effects, J. Chem. Phys. 44 (1966) 154–168, https://doi.org/10.1063/1.1726439.
[30] F. Neese, The ORCA program system, WIREs Comput. *Mol. Sci.* 2 (2012) 73–78, https://doi.org/10.1002/wcms.81.
[31] S.K. Misra, Multifrequency Aspects of EPR, in: S.K. Misra (Eds), Multifrequency Electron Paramagnetic Resonance. Theory and Applications. Wiley-VCH Verlag & Co. KGaA, Boschstr. 12, 69469 Weinheim, Germany, 2011. Pp 23-55. https://onlinelibrary.wiley.com/doi/pdf/10.1002/9783527633531
[32] M. Chakraborty, T. Ahmed, R.S. Dhale, D. Majhi, M. Sarkar, Understanding the microscopic behavior of binary mixtures of ionic liquids through various spectroscopic techniques, J. Phys. Chem. B 122 (2018) 12114–12130, https://doi.org/10.1021/acs.jpcb.8b09699.
[33] E. Quijada-Maldonado, S. van der Boogaart, J.H. Lijbers, G.W. Meindersma, A.B. de Haan, Experimental densities, dynamic viscosities and surface tensions of the ionic liquids series 1-ethyl-3-methylimidazolium acetate and dicyanamide and their binary and ternary mixtures with water and ethanol at T = (298.15 to 343.15 K), J. Chem. Thermodynamics 51 (2012) 51–58, https://doi.org/10.1016/j.jct.2012.02.027.
[34] E. Rilo, J. Vila, M. Garcia, L.M. Varela, O. Cabeza, Viscosity and electrical conductivity of binary mixtures of CnMIM-BF4 with ethanol at 288 K, 298 K, 308 K, and 318 K, Chem. Eng. Data 55 (2010) 5156–5163, https://doi.org/10.1021/je100687x.
[35] J. Hunger, A. Stoppa, S. Schrödle, G. Hefter, R. Buchner, Temperature dependence of the dielectric properties and dynamics of ionic liquids, R, Buchner, ChemPhysChem. 10 (4) (2009) 723–733, https://doi.org/10.1002/cphc.200800483, In this issue.
[36] S.F. Nelsen, Heterocyclic radical anions. II. Naphthalic and 1,4,5,8-naphthalenetetra carboxylic acid derivatives, J. Am. Chem. Soc. 89 (1967) 5925–5931, https://doi.org/10.1021/ja00999a032.
[37] A. Nayeem, S.B. Rananavare, V.S.S. Sastry, J.H. Freed, Heisenberg spin exchange and molecular diffusion in liquid crystals, J. Chem. Phys. 91 (1989) 6887–6905, https://doi.org/10.1063/1.457358.
[38] M.P. Eastman, R.G. Kooser, M.R. Das, J.H. Freed, Studies of Heisenberg spin exchange in ESR spectra. I. Linewidth and saturation effects, J. Chem. Phys. 51 (1969) 2690–2709, https://doi.org/10.1063/1.1672395.
[39] B. Bernert, D. Kivelson, The electron spin resonance line width method for measuring diffusion, A Critique. *J. Phys. Chem.* 83 (1979) 1406–1412, https://doi.org/10.1021/j100474a012.
[40] A.L. Sturlaugson, K.S. Fruchey, M.D. Fayer, Orientational dynamics of room temperature ionic liquid/water mixtures: Water-induced structure, J. Phys. Chem. B 116 (2012) 1777–1787, https://doi.org/10.1021/jp209942r.